Catalytic Microtubular Jet Engines Self-Propelled by Accumulated Gas Bubbles**

Alexander A. Solovev, Yongfeng Mei, Esteban Bermúdez Ureña, Gaoshan Huang, and Oliver G. Schmidt*

***S**train-engineered microtubes with an inner catalytic surface serve as self-propelled microjet engines with speeds of up to ≈2 mm s^{-1} (approximately 50 body lengths per second). The motion of the microjets is caused by gas bubbles ejecting from one opening of the tube, and the velocity can be well approximated by the product of the bubble radius and the bubble ejection frequency. Trajectories of various different geometries are well visualized by long microbubble tails. If a magnetic layer is integrated into the wall of the microjet engine, we can control and localize the trajectories by applying external rotating magnetic fields. Fluid (i.e., fuel) pumping through the microtubes is revealed and directly clarifies the working principle of the catalytic microjet engines.*

Keywords:
- bubbles
- catalytic motion
- jet engines
- nanotechnology

1. Introduction

Catalytic micro- and nanomachines can self-propel by converting chemical fuels (e.g., hydrogen peroxide) from a local environment into kinetic energy.[1–3] Movement in a fluid at low Reynolds numbers[4] is crucial to understand locomotion on the micro- and nanoscale, including biological and molecular motors.[4–8] Substantial effort has therefore been dedicated to developing and understanding catalytic autonomous micro- and nanosystems[1–3,5–8] involving compositions and shapes of catalysts,[1–3,9–12] types of chemical fuels,[13,14] cargo functionality,[15,16] magnetic remote control,[17] and on-chip integration.[16] However, motions in opposite directions were found in otherwise similar multimetallic systems, which were independently explained by interfacial tension gradients[2,18,19] and gas bubble propulsion[1,3]. The former explanation has stimulated other ''non-bubble-recoiling'' mechanisms such as self-electrophoresis[20] and self-diffusiophoresis.[21] Here, we demonstrate a catalytic microjet engine with a speed of up to ≈2 mm s^{-1} (approximately 50 body lengths per second), self-propelled by highly accumulated gas bubbles. We engineer a rolled-up microtube with an inner catalytic surface, serving both as the chemical reaction chamber as well as the gas-collecting cavity. The moving direction is influenced by the tube shape asymmetry along the axis, and the motion can be magnetically controlled if a ferromagnetic layer (Fe/Co) is integrated into the tube wall. We find that the bubble radius is inversely proportional to the bubble generation frequency, and a larger bubble propels the rolled-up microtube over a longer distance. The moving velocity is almost equal to the product of the bubble radius and frequency. The trajectories of the microjet engines are well visualized by the long microbubble tails left behind and reveal various complex geometries. Circular trajectories of microjets are deterministically controlled by tuning the jet velocity or the frequency of the applied rotating magnetic filed. These results suggest that control over directional movement might become feasible in more advanced future micrometer-sized vehicles by simple layer engineering. The mechanism of fluid (i.e., fuel) pumping through the rolled-up engine is revealed, which clarifies the working principle of the catalytic microjet engines.

[*] Dr. Y. F. Mei, A. A. Solovev, E. Bermúdez Ureña, Dr. G. S. Huang, Prof. O. G. Schmidt
Institute for Integrative Nanosciences, IFW Dresden
Helmholtzstr. 20, 01069 Dresden (Germany)
E-mail: y.mei@ifw-dresden.de

Supporting Information is available on the WWW under http://www.small-journal.com or from the author.

DOI: 10.1002/smll.200900021

2. Results and Discussion

The generation of micro- and nanobubbles by rolled-up nanotubes was suggested in Reference [22], and a suitable

NANO MICRO small

technology to create bubbles in hollow catalytic structures was demonstrated recently.[23] The fabrication procedure for the catalytic microtubular jets described here is schematically outlined in Figure 1a. A pre-stressed, multimetallic thin film deposited onto a sacrificial photoresist layer is released from the substrate surface by etching away the photoresist. The layer then spontaneously rolls up and forms into a microtube. The microtube consists of a Pt inner layer used as the catalyst, an Fe layer for magnetic remote control, and a Ti and Au layer for good attachment between layers and for a well-controlled rolling process. Figure 1b displays an optical image of a rolled-up multimetallic microtube, and the corresponding scanning electron microscopy (SEM) image is shown in Figure 1c. This 100-μm-long microtube has a diameter (D) of 5.5 μm and more than 5 windings, which is derived from the rolling distance and tube diameter. The diameter, number of windings, and length of our rolled-up multimetallic microtubes are set by deposition parameters (e.g., film thickness and strain) and lithographically predefined patterns.[23] By immersing a catalytic microtube (still fixed to the substrate surface) into a H_2O_2 solution, microbubbles are generated inside the tube and are ejected with a certain frequency from one of the tube openings (see optical image in the inset of Figure 1d). The mechanism relies on the catalytic decomposition of H_2O_2 into gaseous O_2 and water at the inner surface of the tube wall.

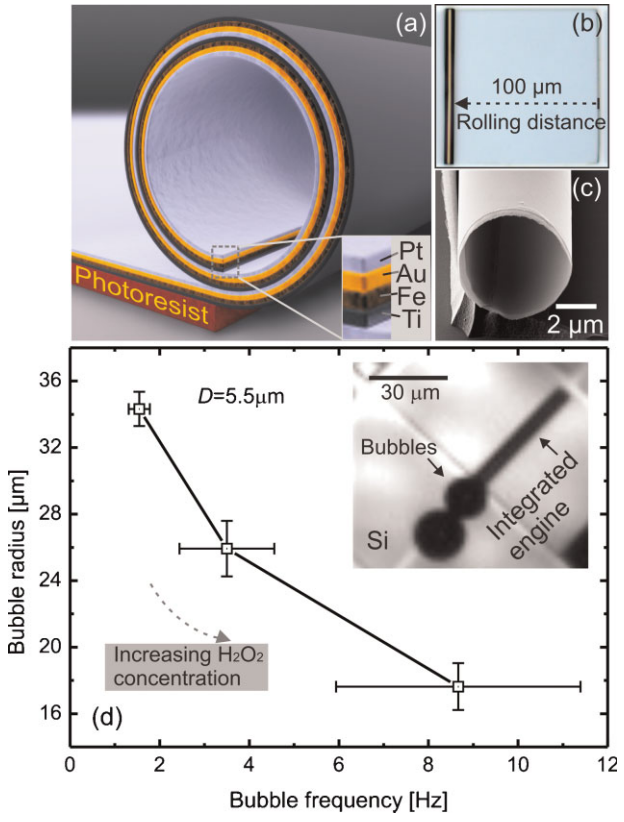

Figure 1. a) Schematic diagram of a rolled-up microtube consisting of Pt/Au/Fe/Ti multilayers on a photoresist sacrificial layer. b) Optical microscopy and c) SEM images of a rolled-up Pt/Au/Fe/Ti microtube. d) Bubble radius as a function of the bubble frequency with increasing H_2O_2 concentration (from 3% to 15%). The inset shows an optical image of an integrated rolled-up microjet engine generating bubbles.

The bubble radius (R) over bubble generation frequency (f) is plotted in Figure 1d. Since it was difficult to quantify exactly the H_2O_2 concentration due to evaporation and reaction consumption, we qualitatively increased the H_2O_2 concentration (from 3% to 15%) to tune the bubble generation frequency of the catalytic engine. As shown in Figure 1d, the bubble radius drops with increasing H_2O_2 concentration, while the frequency increases at the same time by almost an order of magnitude. The gas is produced by the catalytic reaction inside the system, which differs from other methods of bubble generation, in which T-junctions or flow-focusing on externally applied gas sources are used.[24] In our static case (as opposed to the moving one) the bubble radii mostly depend on the pressure difference (ΔP) between the generated gas and environment. This balance can be expressed by $R = 2\gamma/\Delta P$, where γ is the surface tension of the fluid. When the reaction in the tube is accelerated by increasing the H_2O_2 concentration, the generated gas bubbles experience a higher pressure and become smaller in radius. Since the ejection rate is also enhanced by the higher H_2O_2 concentration, the bubble frequency becomes higher as well.

When a rolled-up catalytic microtube is removed from the substrate, it is propelled by a recoiling mechanism produced by expelled microbubbles as shown in Figure 2a. The bubbles collect the gas inside the tube, expand, and then move to the larger opening, where they thrust the tube as they leave. This effect propels the tube by one step, which can be explained as follows: In general, a liquid slug placed in an open conical tube moves up to the end with a smaller diameter due to the difference in Laplace pressure between both menisci of such liquid slugs in a channel.[25,26] The mechanism is vice versa for the gas slug (i.e., bubble) in the microtube as shown in

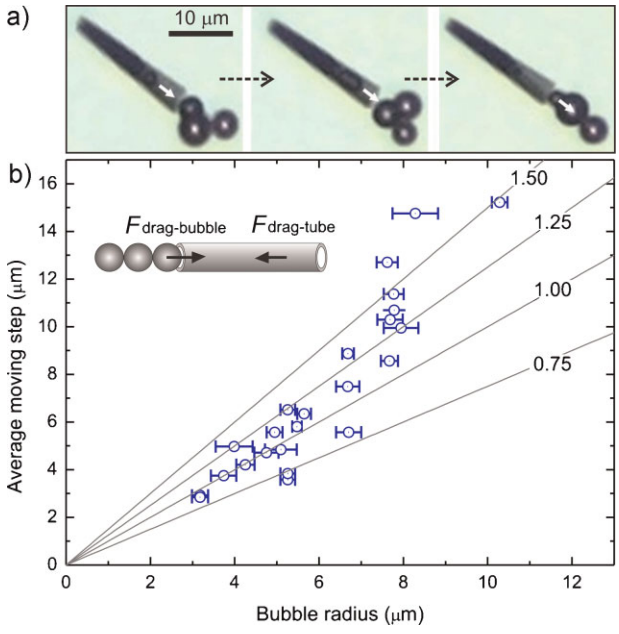

Figure 2. a) From left to right: Generation of a single bubble inside a tubular catalytic microjet. b) Average moving step of catalytic microjets as a function of the bubble radius. The straight lines represent various slopes as references. Driving forces applied to the bubble–tube system are sketched in the inset.

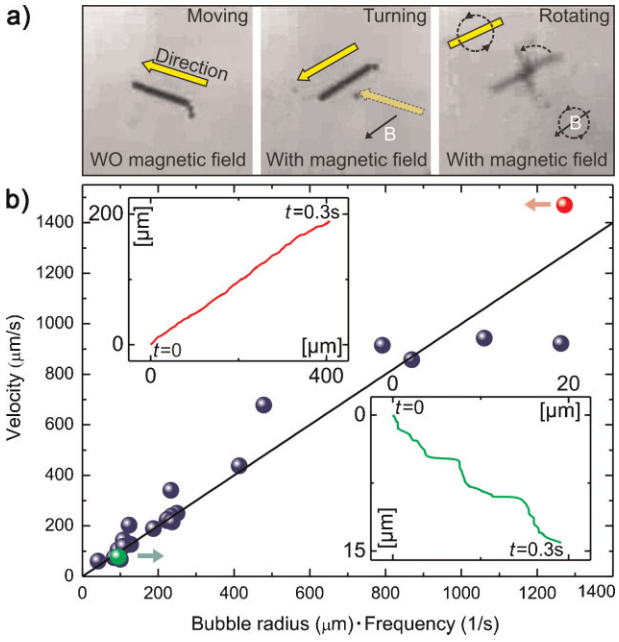

Figure 3. a) Remote control of a catalytic microjet by applying an external magnetic field, thus turning and rotating the jet. b) Statistic data for the microjet velocity as a function of the product of the bubble radius and frequency. The upper-left inset displays a straight trace of a fast jet and the lower-right inset shows another moving trace from a microjet with a lower speed.

Figure 2a, where the gas bubble moves to the large end of the tube.

The moving steps change with varying bubble radii in different microtubes, as presented in Figure 2b. The straight lines represent different ratios of moving step to bubble radius. For small bubble radii (<7 μm), the average moving steps of the jets are almost equal to that of each bubble radius; which means that the drag forces (F_{drag}) on tubes and bubbles are similar. However, when the bubble radius increases, the moving steps become larger than the bubble radius. Since F_{drag} is proportional to the project frontal area,[27] the drag force acting on the bubbles ($F_{drag-bubble}$) becomes larger than the drag force acting on the tube ($F_{drag-tube}$). Hence, when larger bubbles are generated (>7 μm), longer moving steps are observed.

When a magnetic Fe layer is integrated into the rolled-up microtube, an external magnetic field (B) can easily turn or rotate these objects as shown in Figure 3a. A similar effect has been demonstrated by Sen and co-workers for remote-controlled autonomous catalytic motion.[17] The left image in Figure 3a shows a catalytic jet moving in a straight line without (WO) a magnetic field. When a static magnetic field is applied, the catalytic microjet changes direction (middle image), and rotates when a rotating magnetic field is applied (right image). A unidirectional autonomous movement would be desirable for remotely controlled and deterministic motions (a detailed demonstration is described in the following text and Figure 5). Our microjets could be helpful in this respect due to their unique tubular structures, which provide a highly anisotropic distribution of drag forces along the axial and radial directions. As shown in the upper left inset of Figure 3b, a rolled-up catalytic microjet (diameter: 5.5 μm; length: 60 μm) moves unidirectionally with a high velocity of approximately 1.47 mm s^{-1} (≈20 body lengths per second). It is noted that the fastest microjet (≈2 mm s^{-1}) we can obtain is not presented here because it is hard to determine individual bubbles, as shown in the Supporting Information. We performed statistical analysis of the velocities of microjets with various rolled-up catalytic tubes, as displayed in Figure 3b. Due to the material properties (e.g., activity of Pt catalyst) and H_2O_2 concentrations used, the velocity varies from several tens of micrometers up to a couple of millimeters per second. Surprisingly, the velocity is almost equal to the product of the bubble radius and frequency. Slight deviations from the straight line can be explained by bubble collisions or Brownian motion imposed by the environment. The motion of the microjets is strongly influenced by, for example, speed, tubular geometry, and environment. For example, a small tube (diameter: 7.3 μm; length: 80 μm) travels at a speed of approximately 75 μm s^{-1} (around one body length per second) and leaves a more irregular trace behind, which is illustrated in the lower right inset of Figure 3b.

Figure 4 shows various trajectories visualized by the generated microbubble tails of the catalytic microjets. The microbubble tails directly reveal trajectories for a) straight, b) curved, c) circular, d) spiral, and e) self-rotating motions. The geometries of the trajectories are given by the size and shape of the rolled-up microtubes as well as the catalytic machine powers. Similar motions of bacteria have been discussed in a detailed kinematic picture for *Listeria monocytogenes* propelled by actin comet tails.[28]

Full control over microengine motions is required especially for integration in lab-on-a-chip applications. As

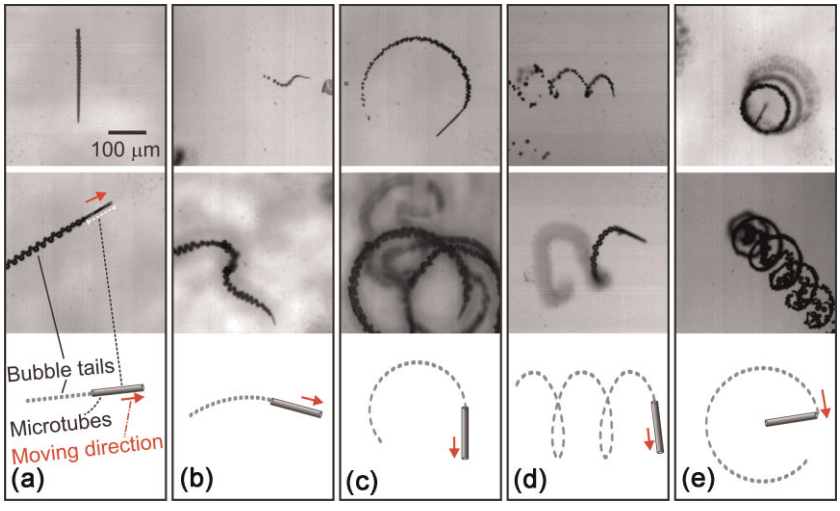

Figure 4. Microbubble tails visualizing trajectories for a) straight, b) curved, c) circular, d) spiral, and e) self-rotating motions of catalytic microjets. The lower schematic diagrams sketch the corresponding moving behaviors.

NANO MICRO small

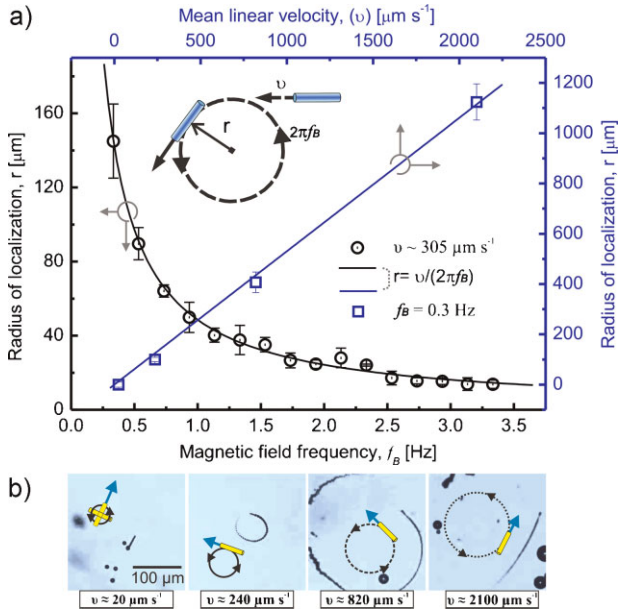

Figure 5. Magnetic control of microjets, which self-propel originally in straight trajectories. a) Localization radius as a function of rotating magnetic-field frequency at a constant linear velocity (black circles) and dependence of localization radius on the mean linear velocity under a constant rotating magnetic field (blue squares). The solid lines are calculations. b) Experimental video frames of a moving microjet at different speeds. Their frames correspond to the data points (blue squares) in (a). Yellow drawings with attached blue arrows represent moving microjets. Black circles with arrows schematically illustrate the applied rotating magnetic field.

an example, we exert control over circular motions (i.e., circular trajectories) of microjets under an external rotating magnetic field. Microjets moving autonomously in straight lines (velocity: υ) start to localize in circular trajectories with radius (r) when a rotating magnetic filed is applied with a constant frequency (f_B) as schematically shown in the inset of Figure 5. Figure 5a (black circle) shows experimental data points of how the localization radius of a microjet moving at constant linear velocity (average value 305 μm s^{-1}) depends on the magnetic-field rotation frequency. The highest sensitivity to a change in localization radius is found in the lower-frequency regime. Blue squares in Figure 5a and frames in Figure 5b show the localization radius as a function of linear velocity for a constant rotating frequency of the magnetic field ($f_B = 0.3$ Hz). The localization radius can be described as a function of the linear velocity and the frequency of the rotating magnetic field: $r = \upsilon/(2\pi f_B)$. For an average linear velocity of 305 μm $s^{-1}$and magnetic-field frequencies in the range of 0.3–3.3 Hz, the calculated black line in Figure 5a well describes the experimental data. For a constant magnetic-field frequency, the localization radius linearly depends on the velocity as plotted by a blue line in Figure 5a, which again well describes our experimental data. However, at higher magnetic-field frequencies the microjets start to hit their own tails (i.e., bubbles), which causes fluctuations in their linear and angular velocities. Our results mimic the behavior of magnetotactic bacteria in rotating magnetic fields. Such bacteria contain nanomagnets and navigate by taking advantage of the relatively week magnetic field of the Earth.[29]

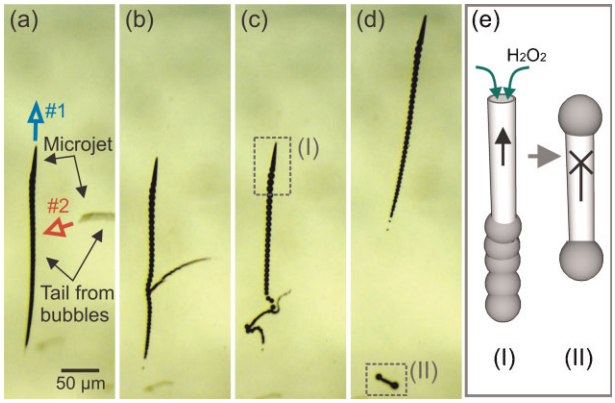

Figure 6. Collision between one microjet and the bubble tail of another, recorded stepwise from (a) to (d). (See text for details.) e) Fuel-pumping mechanism, which ceases once the leading end of the tube becomes blocked by a large bubble.

The rolled-up tubular microjets are self-propelled by the recoil mechanism of accumulated gas bubbles in their catalytic "cavities". Here, we show that the catalytic reaction is fed by fuel entering through the front end of the microjet. In Figure 6, the mechanism for the fuel pumping of the jets is revealed by a collision between one microjet and the bubble tail of another. The first microjet (Jet #1), autonomously moves in one direction, leaving a dense bubble tail behind (Figure 6a). The second microjet (Jet #2) carries out a curved path (Figure 6a), and hits the bubble tail from Jet #1 (Figure 6b). This collision causes a blockage of the front end of Jet #2 by a large bubble (Figure 6c) and the fuel supply ceases, hence immediately stopping the motion of Jet #2 (d). The mechanism is schematically shown in Figure 6e. When a catalytic microjet is self-propelled by the exhaust of accumulated bubbles, the fuel is pumped into the tube front end (case I). Once a bubble attaches to and blocks the leading end (case II), the pumping cycle stops, and the movement halts.

3. Conclusions

We have engineered catalytic tubular microjet engines with speeds of up to ≈2 mm s^{-1} (approximately 50 body lengths per second). The microjets are self-propelled by the recoiling of highly accumulated gas microbubbles and can move unidirectionally. The bubble generation behavior is analyzed systematically as a function of bubble size and generation frequency. Both parameters influence the velocity of the jets. A sandwiched Fe layer enables us to remotely control the motility direction of the catalytic microjets. Moving trajectories, which can be controlled by applying a rotating magnetic field (for example, circular motions), are directly visualized by long microbubble tails and the trajectories resemble those of other biological systems. Our experiments show that the fuel (H_2O_2 solution) is pumped into the front end of the jet engines, while bubbles are generated at the opposite end and thus accelerate the microjets. Our work shows that rolled-up microtubular jet engines are well suited to obtain deeper insight into the working mechanism of catalytic

micro-and nanomachines as well as to exert better control over the direction[7,17] and speed[12] of their motion.

4. Experimental Section

Ti/Fe(Co)/Au/Pt microjets were fabricated by e-beam deposition of metallic layers onto lithographically patterned photoresist layers (experimentally Ti/Fe/Au/Pt used in Figures 1–4, and 6 and Ti/Fe/Co/Pt in Figure 5). Square or circular photoresist patterns with sizes 10–100 μm were prepared on 1.5-inch silicon wafers. Photoresist AR-P 3510 was spin-coated onto silicon wafers at 3500 rpm for 35 s, followed by a soft bake using a hotplate at 95 °C for 1 min and exposure to UV light with a Karl Suss MA56 Mask Aligner (410-605 nm). Patterns were developed in a 1:1 AR300-35:H_2O solution. On-chip rolled-up catalytic microtubes were obtained by a tilted deposition with angles from 50° to 75°, [23] which was used for the experiment of the integrated engine. By dissolving the photoresist layer in acetone solution, pre-stressed multilayers automatically roll up into microtubes. The supercritical point dryer was adopted in the fabrication of rolled-up microtubes to avoid the tube collapsing due to the surface tension of the aqueous etchants. In order to self-propel catalytic microjets, aqueous hydrogen peroxide solutions with concentrations ranging from 3–30% were used as chemical fuels, in which small amounts of isopropanol, surfactants such as benzalkonium chloride solution (from Fluka Chemika), or even common soaps, were added to reduce the surface tension. [30] The microtube morphology was investigated by a Zeiss NVision40 SEM. Under an optical microscope still images were captured by a Zeiss Axiocam MRc camera and live videos were recorded by using a high-speed camera Zeiss Axiocam HSm generating 200 frames per second.

Acknowledgements

We are grateful for the assistance of Ronny Engelhard, Elliot John Smith, and Emica Coric.

[1] R. F. Ismagilov, A. Schwartz, N. Bowden, G. M. Whitesides, *Angew. Chem. Int. Ed.* **2002**, *41*, 652–654.
[2] W. F. Paxton, K. C. Kistler, C. C. Olmeda, A. Sen, S. K. St. Angelo, Y. Cao, T. E. Mallouk, P. E. Lammert, V. H. Crespi, *J. Am. Chem. Soc.* **2004**, *126*, 13424–13431.
[3] S. Fournier-Bidoz, A. C. Arsenault, I. Manners, G. A. Ozin, *Chem. Comm.* **2005**, 441–443.
[4] E. M. Purcell, *Am. J. Phys.* **1977**, *45*, 3–11.
[5] G. A. Ozin, I. Manners, S. Fournier-Bidoz, A. Arsenault, *Adv. Mater.* **2005**, *17*, 3011–3018.
[6] W. F. Paxton, S. Sundararajan, T. E. Mallouk, A. Sen, *Angew. Chem. Int. Ed.* **2006**, *45*, 5420–5429.
[7] a) W. R. Browne, B. L. Feringa, *Nat. Nanotech.* **2006**, *1*, 25–35; b) C. Stock, N. Heureux, W. R. Browne, B. L. Feringa, *Chem.-Eur. J.* **2008**, *14*, 3146–3153.
[8] E. R. Kay, D. A. Leigh, F. Zerbetto, *Angew. Chem. Int. Ed.* **2007**, *46*, 72–191.
[9] Y. Wang, R. M. Hernandez, D. J. Bartlett, Jr., J. M. Bingham, T. R. Kline, A. Sen, T. E. Mallouk, *Langmuir* **2006**, *22*, 10451–10456.
[10] a) Y. He, J. Wu, Y. Zhao, *Nano Lett.* **2007**, *7*, 1369–1375; b) N. I. Kovtyukhova, *J. Phys. Chem. C* **2008**, *112*, 6049–6056.
[11] L. Qin, M. J. Banholzer, X. Xu, L. Huang, C. A. Mirkin, *J. Am. Chem. Soc.* **2007**, *129*, 14870–14871.
[12] R. Laocharoensuk, J. Burdick, J. Wang, *ACS Nano* **2008**, *2*, 1069–1075.
[13] N. Mano, A. Heller, *J. Am. Chem. Soc.* **2005**, *127*, 11574–11575.
[14] D. Pantarotto, W. R. Browne, B. L. Feringa, *Chem. Comm.* **2008**, 1533–1535.
[15] S. Sundararajan, P. E. Lammert, A. W. Zudans, V. H. Crespi, A. Sen, *Nano Lett.* **2008**, *8*, 1271–1276.
[16] J. Burdick, R. Laocharoensuk, P. M. Wheat, J. D. Posner, J. Wang, *J. Am. Chem. Soc.* **2008**, *130*, 8164–8165.
[17] T. R. Kline, W. F. Paxton, T. E. Mallouk, A. Sen, *Angew. Chem. Int. Ed.* **2005**, *44*, 744–746.
[18] W. F. Paxton, P. T. Baker, T. R. Kline, Y. Wang, T. E. Mallouk, A. Sen, *J. Am. Chem. Soc.* **2006**, *128*, 14881–14888.
[19] N. B. Saidulu, K. L. Sebastian, *J. Chem. Phys.* **2008**, *128*, 074708.
[20] W. F. Paxton, A. Sen, T. E. Mallouk, *Chem. Eur. J.* **2005**, *11*, 6462–6470.
[21] J. R. Howse, R. A. L. Jones, A. J. Ryan, T. Gough, R. Vafabakhsh, R. Golestanian, *Phys. Rev. Lett.* **2007**, *99*, 048102.
[22] O. G. Schmidt, K. Eberl, *Nature* **2001**, *410*, 168.
[23] Y. F. Mei, G. S. Huang, A. A. Solovev, E. Bermúdez Ureña, I. Mönch, F. Ding, T. Reindl, R. K. Y. Fu, P. K. Chu, O. G. Schmidt, *Adv. Mater.* **2008**, *20*, 4085–4090.
[24] S.-Y. The, R. Lin, L.-H. Hung, A. P. Lee, *Lab Chip* **2008**, *8*, 198–220.
[25] J. Bico, D. Quere, *J. Fluid Mech.* **2002**, *467*, 101–127.
[26] J. C. T. Eijkel, A. V. D. Berg, *Lab Chip* **2005**, *5*, 1202–1209.
[27] P. Snabre, F. Magnifotcham, *Eur. Phys. J. B* **1998**, *4*, 369–377.
[28] V. B. Shenoy, D. T. Tambe, A. Prasad, J. A. Theriot, *Proc. Natl. Acad. Sci. U. S. A.* **2007**, *104*, 8229–8234.
[29] K. Ērglis, Q. Wen, V. Ose, A. Zeltins, A. Sharipo, P. A. Janmey, A. Cēbers, *Biophys. J.* **2007**, *93*, 1402–1412.
[30] Catalytic microtubes consisting of thin metal layers are not eager to mix with the aqueous solution of hydrogen peroxide because of their hydrophobicity. Fuel solutions were prepared in a mixture of different concentration of hydrogen peroxide with small amount of isopropanol, surfactants like benzalkonium chloride solution (from Fluka Chemika), or even common soaps (from Fit GmbH; components: 5–15% anionic tenside (5–15%), amphoteric tenside (<5%), Bronopol, Benzisothiazolinone, Methylisothiazolinone), which could reduce the surface tension. Soaps might also stabilize microbubbles, and thus leading to improved propulsions. One similar effect of the fluid surface tension on catalytic motions has been demonstrated by: J. M. Catchmark, S. Subramanian, A. Sen, *Small* **2005**, *1*, 202–206.

Received: January 6, 2009
Revised: February 18, 2009
Published online: April 16, 2009

